International Journal of Solids and Structures 46 (2009) 2093–2110

Contents lists available at ScienceDirect

International Journal of Solids and Structures

journal homepage: www.elsevier.com/locate/ijsolstr

Flexure analysis of unsymmetric orthotropic beams with an interlayer

K.S. Alfredsson [a,*], J.W. Gillespie Jr. [b], L.A. Carlsson [c], T.A. Bogetti [d], A. Yiournas [e]

[a] University of Skövde, Division of Mechanical Engineering, P.O. Box 408, S-541 28 Skövde, Sweden
[b] Center for Composite Materials, Department of Civil and Environmental Engineering and Department of Materials Science and Engineering, University of Delaware, Newark, DE 19716, USA
[c] Department of Mechanical Engineering, Florida Atlantic University, Boca Raton, FL 33431, USA
[d] Army Research Laboratory, Aberdeen Proving Ground, MD 21005, USA
[e] Dynamic Science Inc. DTSD, Aberdeen, MD 21001, USA

ARTICLE INFO

Article history:
Received 23 January 2008
Received in revised form 18 July 2008
Available online 7 August 2008

Keywords:
Beam
Bending
Layers
Material combination
Rubbers
Shear deformation

ABSTRACT

This paper presents a layer-wise stress and deformation analysis of a three-layer beam configuration consisting of two dissimilar orthotropic adherends of different thicknesses that are joined together by a deformable interlayer of finite thickness. Analytical solutions for the case of three-point flexure loading are presented for both compressible and incompressible interlayers. Parametric analysis reveals the influences of asymmetry of moduli and adherend thicknesses, interlayer thickness, and overhang of the beams on the beam compliance. Analytical predictions of beam compliance show very good agreement with finite element results. Experimental measurements of compliance of various unsymmetric beams consisting of aluminum adherends separated by a rubber interlayer were performed in order to validate the analysis. Excellent agreement between measured and predicted compliance values was observed.

1. Introduction

Numerous applications can benefit from the incorporation of shear-deformable interlayers by tailoring load paths, providing energy dissipation and controlling overall structural deformation. Mahdi and Gillespie (2004) have shown that a compliant interlayer in protective armor can effectively decouple the ceramic strike face from the composite backing plate to limit tensile stress in the ceramic that can cause premature structural failure while at the same time improving energy dissipation. Recently, there has been increasing interest in the automotive industry in replacing steel leaf springs with composite leaf springs. It has been found that a thin rubber interlayer undergoing intense shear deformation improves the damping in such springs (Kristensen et al., 2008).

Design of structures containing a shear-deformable interlayer requires a firm understanding of the role of thicknesses of the adherends and the thickness and stiffness of the interlayer in its ability to moderate the static and dynamic behaviors of the structure. Most analysis of beam and plate elements of such structures to date are based on finite element analysis, see Davila and Chen (2000) and Mahdi and Gillespie (2004), since it is widely recognized that the large local shear deformation of the layer prohibits the use of ordinary beam and plate theories (Gere and Timoshenko, 1984; Timoshenko and Woinowsky-Krieger, 1959) and first-order shear deformation theory (Whitney, 1987). Reddy (1984) presented a higher-order theory that has gained much acceptance and implementation in a finite element formulation by Nayak et al. (2004). This formulation is an effective single-layer plate theory which does not allow specification of boundary conditions for the individual layers. More recently, Hohe et al. (2006) presented higher-order analysis of sandwich structures that includes the effect of

* Corresponding author. Tel.: +46 500 448526; fax: +46 500 448599.
E-mail address: svante.alfredsson@his.se (K.S. Alfredsson).

0020-7683/$ - see front matter © 2008 Elsevier Ltd. All rights reserved.
doi:10.1016/j.ijsolstr.2008.07.024

transverse compressibility of the core. Again, the theory emphasizes the overall structural response of the sandwich. Proper analysis of structures with a flexible interlayer demands layer-wise theories such as the one pioneered by Frostig et al. (1991, 1992). They developed a superposition analysis to determine the effects of transverse flexibility of the core in sandwich beams with a thick flexible core. A more recent review article by Frostig (2003) presents a comparison between classical shear deformation analysis, elastic foundation models, and higher-order layerwise analysis based on variational principles.

The present work is an extension of the analysis of a symmetric beam configuration presented in an earlier paper by Alfredsson et al. (2008). The aim is to develop a model of the global bending behavior of unsymmetric sandwich beams. The intention is not to study local phenomena. The approach is similar to the model presented by Frostig et al. (1991) although we use a direct solution technique that bypasses their intricate superposition solution. It will be shown that our solution displays a more complex interaction between peel and shear stresses in the flexible interlayer than indicated by the superposition analysis of Frostig et al. (1991).

2. Governing equations

Similar to an earlier paper by the authors (Alfredsson et al., 2008), we will specifically consider a three-point flexure loaded layered beam with adherends labeled # 1 (top) and bottom (# 2) joined by a flexible interlayer of thickness, t, see Fig. 1. The span length is L and the overhang length is c. The x coordinate is zero at the left support. The layer-wise approach used in the earlier paper (Alfredsson et al., 2008) is extended to the unsymmetric beam configuration.

The adherends are assumed to deform according to classical beam theory, i.e. plane cross-sections remain plane and perpendicular to the adherend axis. The displacements of the adherends are described by the longitudinal and vertical displacements of the adherends' centroids, u_i and w_i ($i = 1, 2$), respectively. Thus, the longitudinal displacements are assumed to vary linearly across the thickness of the top and bottom layers of the beam. The thickness change of the adherends is considered negligible as compared to the thickness change of the flexible interlayer. Hence, the vertical displacements of the adherends are assumed to be constant across the thickness of the top and bottom layers of the beam. The interlayer is assumed to have a stiffness which is orders of magnitude smaller than the stiffness of the adherends. Thus, the longitudinal stiffness of the interlayer can be neglected. This means that longitudinal equilibrium is fulfilled by a shear stress, τ, which is constant through the thickness of the interlayer. In order to fulfil vertical equilibrium, the peel stresses at the upper and lower edges of the interlayer, σ_1 and σ_2, must be different for the case of a varying shear stress, see Fig. 2. The interlayer is allowed to deform in peel and shear and is assumed to be linearly elastic. This means that the variation across the thickness of the interlayer is assumed to be linear for the longitudinal displacements and quadratic for the vertical displacements.

The modeling approach shares several elements with the classical solution for adhesive joints with an infinitesimally thin compliant adhesive layer originally presented by Goland and Reissner (1944) and subsequently further developed by several authors (e.g. Cornell, 1953; Hart-Smith, 1973; Bigwood and Crocombe, 1989; Alfredsson and Högberg, 2008). The present solution is an extension to interlayers of finite thickness of the solution presented by Alfredsson and Högberg (2008).

The governing equations are derived by requiring that each of the small elements of the adherends (# 1 and 2) in Fig. 2 are in equilibrium

$$N_1'(x) + b\tau(x) = 0, \quad N_2'(x) - b\tau(x) = 0 \tag{1a,b}$$

$$V_1'(x) + b\sigma_1(x) = 0, \quad V_2'(x) - b\sigma_2(x) = 0 \tag{2a,b}$$

$$V_1(x) = M_1'(x) + \frac{1}{2}bh_1\tau(x), \quad V_2(x) = M_2'(x) + \frac{1}{2}bh_2\tau(x) \tag{3a,b}$$

where b is the width of the beam, h_1 and h_2 are the thicknesses of the adherends, see Fig. 1, and the prime on the axial and shear forces, N_i and V_i, and moments, M_i, indicates differentiation with respect to x.

For the convenience of the subsequent analysis, the normal stresses in the interlayer are divided into symmetric (s) and antisymmetric (a) parts, see Fig. 3

$$\sigma_s = \frac{1}{2}(\sigma_1 + \sigma_2), \quad \sigma_a = \frac{1}{2}(\sigma_1 - \sigma_2) \tag{4a,b}$$

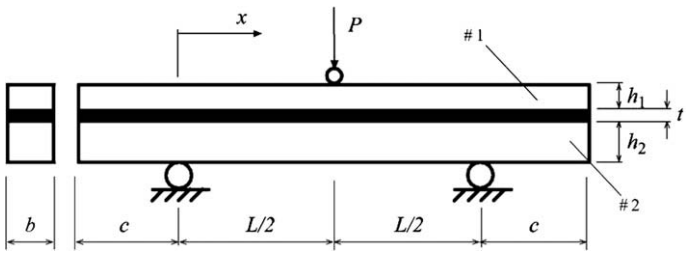

Fig. 1. Three-point flexure loading of unsymmetric beam with symmetric overhangs.

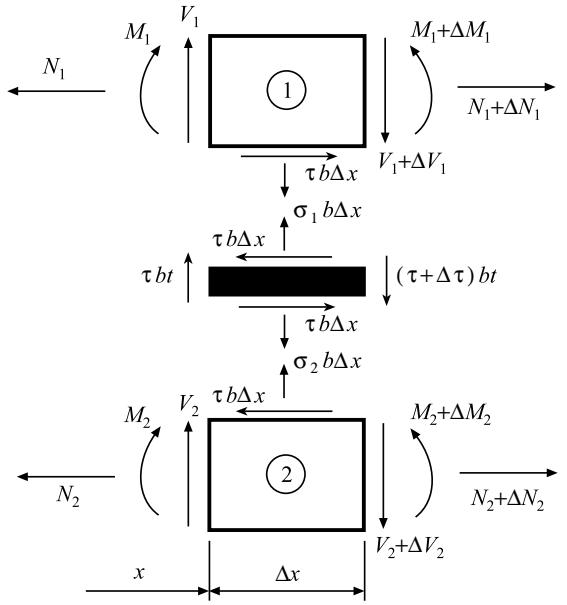

Fig. 2. Positive directions of adhesive stresses and sectional loads.

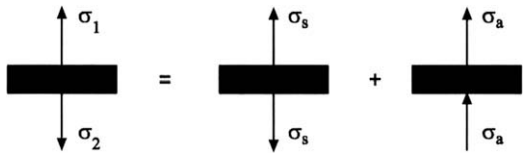

Fig. 3. Superposition of symmetric and antisymmetric stresses on the interlayer.

Hence, the actual stresses are. $\sigma_1 = \sigma_s + \sigma_a$ and $\sigma_2 = \sigma_s - \sigma_a$.

Since the interlayer is considered to have a finite thickness, it will carry part of the total shear force, $\overline{V}$, see Fig. 4. Thus, the shear stress in the interlayer will interact with the normal stresses acting on the top and bottom surfaces of the interlayer to form the vertical equilibrium of the flexible interlayer, Fig. 2

$$2\sigma_a(x) = t\tau'(x) \tag{5}$$

The equilibrium equations are supplemented by the constitutive equations for the elastically deforming adherends. For the case of plane stress they read

$$N_1(x) = E_1 b h_1 u_1'(x), \quad N_2(x) = E_2 b h_2 u_2'(x) \tag{6a, b}$$

$$M_1(x) = -\frac{1}{12} E_1 b h_1^3 w_1''(x), \quad M_2(x) = -\frac{1}{12} E_2 b h_2^3 w_2''(x) \tag{7a, b}$$

where E_1 and E_2 are the Young's moduli of the adherends, which may be isotropic or orthotropic. In this paper the nomenclature refers to isotropic adherends, but the analysis is equally valid for homogeneous orthotropic adherends. The model is not directly applicable for general laminates.

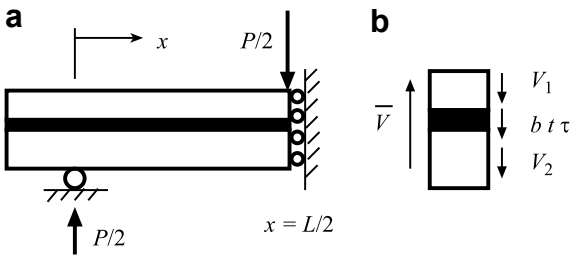

Fig. 4. Symmetry section of three-point flexure specimen (a), and shear forces acting on element of beam (b).

The relative axial and transverse displacements of the beam centers are, Fig. 5

$$u(x) = u_2(x) - u_1(x), \quad w(x) = w_2(x) - w_1(x) \tag{8a, b}$$

where u_1 and u_2 are the horizontal displacements of adherends 1 and 2 (Fig. 5a) and w_1 and w_2 are the deflections of the adherends. It is noted that the relative deflection, w, represents the thickness change of the interlayer, provided that the thickness changes of the adherends are neglected.

The flexibility of the interlayer allows for different rotations (w_1' and w_2') of the two adherends. The rotations and the relative axial displacement, u, contribute to the shear deformation of the layer, v. For the case of zero rotations, the shear deformation equals the relative axial displacement, see Fig. 5a. In order to account for rotations and obtain an expression for the shear deformation, the rotations of the adherends are split into symmetric (s) and antisymmetric (a) parts as illustrated in Fig. 5b and c

$$\phi_s = \frac{1}{2}(w_2' - w_1'), \quad \phi_a = \frac{1}{2}(w_1' + w_2') \tag{9a, b}$$

The actual rotations of the adherends are thus given by $w_1' = \phi_a - \phi_s$ and $w_2' = \phi_a + \phi_s$.

Superposition of the contributions gives the shear deformation

$$v = u_2 - u_1 + \phi_s(h_2 - h_1)/2 + \phi_a(h_1 + h_2 + 2t)/2 \tag{10}$$

From Eqs. (8a) and (9) and (10) the shear deformation of the interlayer becomes

$$v(x) = u(x) + \frac{1}{2}(h_1 + t)w_1'(x) + \frac{1}{2}(h_2 + t)w_2'(x) \tag{11}$$

The solution of the governing equations depends on whether or not the interlayer is compressible. The two cases of (i) a compressible interlayer and (ii) an incompressible interlayer are treated separately in Sections 3 and 4 to follow.

3. Solution for a compressible interlayer

The solution strategy is to first determine a general solution for the deformations of the interlayer, $v(x)$ and $w(x)$, and then derive a general solution for the individual displacements of the adherends, $w_i(x)$ and $u_i(x)$.

3.1. Deformation of the interlayer

The axial displacements of the adherends, u_i and deflections w_i, can be eliminated from Eqs. (1–11), see Appendix A. The result is two differential equations for the relative deflection and shear deformation

$$w^{IV}(x) = 6\left(\frac{1+\frac{t}{h_2}}{E_2h_2^2} - \frac{1+\frac{t}{h_1}}{E_1h_1^2}\right)\tau'(x) - 12\left(\frac{1}{E_1h_1^3} + \frac{1}{E_2h_2^3}\right)\sigma_s(x) \tag{12a}$$

$$v'''(x) = 4\left(\frac{1+\frac{3}{2}\frac{t}{h_1}+\frac{3}{4}\left(\frac{t}{h_1}\right)^2}{E_1h_1} + \frac{1+\frac{3}{2}\frac{t}{h_2}+\frac{3}{4}\left(\frac{t}{h_2}\right)^2}{E_2h_2}\right)\tau'(x) + 6\left(\frac{1}{E_1h_1^2} - \frac{1}{E_2h_2^2}\right)\sigma_s(x) \tag{12b}$$

These equations are independent of the constitutive model for the interlayer.

It is recognized that only the symmetric part of the normal stress, σ_s, contributes to the thickness change of the interlayer, see Fig. 3. For the case of a very thin flexible interlayer it can be shown that it is appropriate to assume zero in-plane layer strains (ε_{xx} and ε_{yy}) of the interlayer (Klarbring, 1991). This implies that an effective Young's modulus, $\bar{E} \geqslant E$, should be used

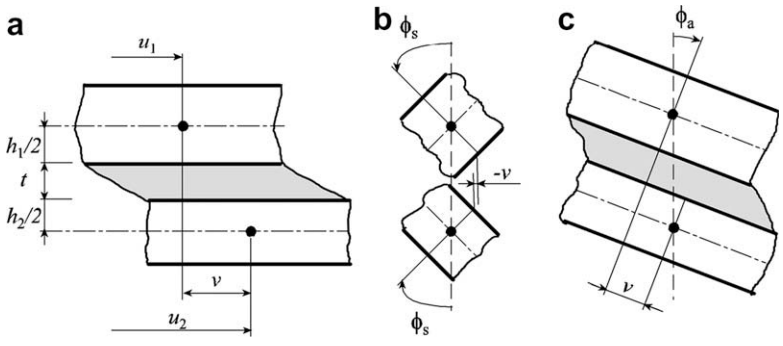

Fig. 5. Shear deformation of flexible layer due to longitudinal displacement (a), symmetric slopes (b) and antisymmetric slopes (c).

for the elongational stiffness. This concept is adopted here also for cases where the interlayer is not thin compared to the adherends. This assumption should be justified by the large mismatch in the stiffnesses of the adherends and the interlayer.

Linear-elastic isotropic behavior of the flexible interlayer is assumed as

$$\tau = \frac{G}{t}v, \quad \sigma_s = \frac{\bar{E}}{t}w \tag{13a, b}$$

where $G = E/[2(1+\nu)]$ and $\bar{E} = E(1-\nu)/[(1-2\nu)(1+\nu)]$ are the shear modulus and the effective Young's modulus of the constrained interlayer (Klarbring, 1991). Here, E is Young's modulus and ν is Poisson's ratio of the interlayer.

Eqs. (12) and (13) yield two coupled differential equations for the relative deflection and the shear deformation

$$w^{IV}(x) - Av'(x) + Bw(x) = 0, \quad v'''(x) - Cv'(x) + Dw(x) = 0 \tag{14a, b}$$

with

$$A = A_2 - A_1, \quad \text{where} \quad A_i = \frac{6G}{E_i h_i^2 t}\left(1 + \frac{t}{h_i}\right) \quad i = 1,2 \tag{15a}$$

$$B = B_1 + B_2, \quad \text{where} \quad B_i = \frac{12\bar{E}}{E_i h_i^3 t} \quad i = 1,2 \tag{15b}$$

$$C = C_1 + C_2, \quad \text{where} \quad C_i = \frac{4G}{E_i h_i t}\left[1 + \frac{3}{2}\frac{t}{h_i} + \frac{3}{4}\left(\frac{t}{h_i}\right)^2\right] \quad i = 1,2 \tag{15c}$$

$$D = D_2 - D_1, \quad \text{where} \quad D_i = \frac{6\bar{E}}{E_i h_i^2 t}\left(1 + \frac{t}{h_i}\right) \quad i = 1,2 \tag{15d}$$

At this point, the original seven parameters $(E_1, E_2, h_1, h_2, G, \bar{E}, t)$ are reduced to four cross-sectional parameters (A, B, C, D). Notice that the ratio $A/D = G/\bar{E}$ is a function of Poisson's ratio (ν) of the interlayer only.

Eq. (14) constitute a system of two coupled ordinary differential equations. The parameters A and D are responsible for the coupling. When $E_1 h_1^2/(1 + t/h_1) = E_2 t_2^2/(1 + t/h_2)$, $A = D = 0$. Such a configuration is denoted *balanced* in the following. All other configurations are denoted *unbalanced*. Depending on the type of system, balanced or unbalanced, the general solution for the deformation of the interlayer takes different forms.

3.1.1. Balanced configuration

For the balanced case, $A = D = 0$ in Eq. (15), only two cross-sectional parameters, B and C, remain. Thus, the differential equations (14) uncouple

$$w^{IV}(x) + Bw(x) = 0, \quad v'''(x) - Cv'(x) = 0 \tag{16a, b}$$

The general solution is

$$w(x) = e^{\kappa_p x}(S_1 \sin \kappa_p x + S_2 \cos \kappa_p x) + e^{-\kappa_p x}(S_3 \sin \kappa_p x + S_4 \cos \kappa_p x) \tag{17a}$$

$$v(x) = S_5 e^{\kappa_s x} + S_6 e^{-\kappa_s x} + S_7 \tag{17b}$$

where S_i ($i = 1, 2, 3, \ldots, 7$) are seven integration constants. The so called wave-numbers κ_p and κ_s are given by

$$\kappa_p^4 = B/4 = \frac{3\bar{E}}{t}\left(\frac{1}{E_2 h_2^3} + \frac{1}{E_1 h_1^3}\right) \tag{18a}$$

$$\kappa_s^2 = C = \frac{4G}{t}\left(\frac{1 + \frac{3}{2}\frac{t}{h_2} + \frac{3}{4}\left(\frac{t}{h_2}\right)^2}{E_2 h_2} + \frac{1 + \frac{3}{2}\frac{t}{h_1} + \frac{3}{4}\left(\frac{t}{h_1}\right)^2}{E_1 h_1}\right) \tag{18b}$$

Thus, for a balanced system, κ_p and κ_s, replace B and C as cross-sectional parameters.

3.1.2. Unbalanced configuration

A general configuration for which $E_1 h_1^2/(1 + t/h_1) \neq E_2 t_2^2/(1 + t/h_2)$ is denoted *unbalanced*. For such a case, however, the two coupled differential equations (14) may be transformed into two uncoupled differential equations of higher-order

$$w^{VI}(x) - Cw^{IV}(x) + Bw''(x) + (AD - BC)w(x) = 0 \tag{19a}$$

$$v^{VII}(x) - Cv^{V}(x) + Bv'''(x) + (AD - BC)v'(x) = 0 \tag{19b}$$

Note the similarity of these two equations. For the relative deflection, w, Eq. (19a), a general solution in the form $w(x) = e^{rx}$ leads to the characteristic equation

$$(r^4 + B)(r^2 - C) + AD = 0 \tag{20}$$

Eq. (20) is a third order equation in r^2, the roots of which may be found in a mathematical handbook, for example (Råde and Westergren, 1990). Two roots are complex and conjugate roots, and one of the three roots is real and non-negative. This results in six roots, r_i, of the form

$$r_{1,2,3,4} = \pm\kappa_1 \pm i\kappa_2, \quad r_{5,6} = \pm\kappa_3 \tag{21a, b}$$

where $\kappa_{1,\,2,\,3}$ are real positive numbers. These roots have units of inverse length (m^{-1}) and represent an inverse length scale of the solution.

For the shear deformation, v, Eq. (19b), the roots of the characteristic equation are the same as in Eq. (21), but an additional root, $r_7 = 0$, appears. The general solutions of Eq. (19) are thus given by

$$\begin{aligned} w(x) &= e^{\kappa_1 x}(\overline{K}_1 \sin\kappa_2 x + \overline{K}_2 \cos\kappa_2 x) \\ &\quad + e^{-\kappa_1 x}(\overline{K}_3 \sin\kappa_2 x + \overline{K}_4 \cos\kappa_2 x) + \overline{K}_5 e^{\kappa_3 x} + \overline{K}_6 e^{-\kappa_3 x} \end{aligned} \tag{22a}$$

$$\begin{aligned} v(x) &= e^{\kappa_1 x}(K_1 \sin\kappa_2 x + K_2 \cos\kappa_2 x) \\ &\quad + e^{-\kappa_1 x}(K_3 \sin\kappa_2 x + K_4 \cos\kappa_2 x) + K_5 e^{\kappa_3 x} + K_6 e^{-\kappa_3 x} + K_7 \end{aligned} \tag{22b}$$

The integration constants, K_{1-6} and $\overline{K}_{1-6}$, are dependent. The relations are found by inserting the general solution, Eq. (22), into one of Eq. (14), which yields

$$\overline{K}_1 = \alpha_1 K_1 - \alpha_2 K_2, \quad \overline{K}_2 = \alpha_2 K_1 + \alpha_1 K_2, \tag{23a, b}$$

$$\overline{K}_3 = -\alpha_1 K_3 - \alpha_2 K_4, \qquad \overline{K}_4 = \alpha_2 K_3 - \alpha_1 K_4, \tag{23c, d}$$

$$\overline{K}_5 = \alpha_3 K_5, \quad \overline{K}_6 = -\alpha_3 K_6 \tag{23e, f}$$

where

$$\alpha_1 = \kappa_1(C - \kappa_1^2 + 3\kappa_2^2)/D, \quad \alpha_2 = \kappa_2(C + \kappa_2^2 - 3\kappa_1^2)/D, \quad \alpha_3 = \kappa_3(C - \kappa_3^2)/D \tag{24a, b, c}$$

Hence, also for the unbalanced case, seven independent integration constants, K_i (i = 1, 2, 3,. . .,7) emerge.

3.2. Displacements of the adherends

The governing equations derived in Section 2 can be used to obtain a solution for the displacements of each of the two adherends, see Appendix B. The following solutions apply to a general unbalanced configuration. The deflections are given by

$$w_1(x) = A_1(B^2 v' - BDw'' - DQw)/Q^2 + B_1(ABv' - ADw'' - CQw)/Q^2 - \frac{1}{12}\frac{\overline{C}L^3}{h_1 + h_2 + 2t}K_7\frac{x^3}{L^3} + I_1\frac{x^2}{L^2} + I_2\frac{x}{L} + I_3 \tag{25a}$$

$$w_2(x) = A_2(B^2 v' - BDw'' - DQw)/Q^2 - B_2(ABv' - ADw'' - CQw)/Q^2 - \frac{1}{12}\frac{\overline{C}L^3}{h_1 + h_2 + 2t}K_7\frac{x^3}{L^3} + I_1\frac{x^2}{L^2} + I_2\frac{x}{L} + I_3 \tag{25b}$$

where $Q = BC - AD$, and the span length, L, has been introduced as a normalizing factor. The axial displacements of the center of each adherend are given by

$$u_1(x) = -\frac{1}{4}\overline{C}_1\left[(Bv - Dw')/Q + \frac{1}{2}K_7 x^2\right] + I_4\frac{x}{L} + I_5 \tag{26a}$$

$$u_2(x) = \frac{1}{4}\overline{C}_2\left[(Bv - Dw')/Q + \frac{1}{2}K_7 x^2\right] + \left(I_4 - \frac{h_1 + h_2 + 2t}{L}I_1\right)\frac{x}{L} + I_5 - \frac{1}{2}\frac{h_1 + h_2 + 2t}{L}I_2 + \left[1 - \frac{1}{4}B\overline{C}/Q\right]K_7 \tag{26b}$$

where

$$\overline{C} = \overline{C}_1 + \overline{C}_2, \quad \text{where} \quad \overline{C}_i = \frac{4G}{E_i h_i t}, \quad i = 1, 2 \tag{27}$$

The solution for a balanced system is obtained by replacing K_7 with S_7 and setting $A = D = 0$ in Eqs. (25) and (26). The expressions for the interlayer deformation, v and w, are given by Eq. (17) (balanced) and (22) (unbalanced). Each of these expressions contain seven integration constants, ($K_{1\,-\,7}$ or $S_{1\,-\,7}$). Five new integration constants $I_{1\,-\,5}$ appear in the expressions for the individual displacements, cf. Eqs. (25) and (26). Thus, the general solution contains 12 independent constants, which are determined from boundary conditions.

It may here be noted that even though the model used in the present paper is similar to the one developed by Frostig et al. (1991), our solution (Eqs. (25) and (26)) displays a more complex interaction between peel and shear stresses in the flexible interlayer.

Boundary conditions in the form of prescribed displacements or rotations, u_i, w_i or w_i', are formed directly from Eqs. (25) and (26). Boundary conditions on axial force and bending moment require that u_i' and w_i'' are prescribed using Eqs. (6) and (7). Boundary conditions involving shear forces are formed by prescribing a combination of w_i''' and v. The result is

$$V_i(x) = -\frac{E_i b h_i^3}{12}[w_i'''(x) - \overline{A}_i v(x)], \quad \overline{A}_i = \frac{6G}{E_i h_i^2 t}, \quad i = 1,2 \tag{28a, b}$$

which follows from Eqs. (3), (7), (13a) and (15a).

3.3. Solution for three-point flexure specimen

3.3.1. Boundary conditions for beams without overhang

Consider first a beam without overhang, i.e., $c = 0$ in Fig. 1. Due to symmetry only the left half of the layered beam, $0 \leqslant x < L/2$, is considered. The deflections and axial displacements of the adherends are given by Eqs. (25) and (26). The solutions for the displacements contain 12 integration constants (K_{1-7} and I_{1-5}). Hence, 12 boundary conditions are needed. Boundary conditions may be formulated by considering the symmetry section of the three-point flexure configuration shown in Fig. 4. Symmetry is modelled by the roller support at $x = L/2$. A load of magnitude $P/2$ is introduced on the top surface at the symmetry section. At this section the lower beam does not carry any shear force, i.e. $V_1(L/2) = P/2$ and $V_2(L/2) = 0$, see Fig. 4. Due to shear and compressive stresses in the interlayer in cross-sections away from $x = L/2$, shear force is transferred from the top beam to the lower beam. Symmetry at $x = L/2$ further requires vanishing of the longitudinal displacements and the slopes, i.e. $u_1 = u_2 = 0$ and $w_1' = w_2' = 0$. Thus, six conditions are imposed at $x = L/2$. The six remaining conditions are formed at the left end ($x = 0$), where N_1, M_1, V_1, N_2, M_2 and w_2 are zero.

3.3.2. Boundary conditions for beams with overhang

Consider next a beam with overhang, i.e. $c > 0$ in Fig. 1. Only the left half symmetry section of the beam, $-c \leqslant x \leqslant L/2$, is considered. The deflections and axial displacements of the adherends are given by Eqs. (25) and (26). The solution contains 24 integration constants; 12 (K_{1-7} and I_{1-5}) for the overhang part, $-c \leqslant x \leqslant 0$, and another 12 for the loaded region, $0 \leqslant x \leqslant L/2$. Thus, the solution requires in total 24 conditions. At the point of load introduction ($x = L/2$), the six boundary conditions are identical to the case without overhang, i.e. $V_1 = P/2$ and u_1, u_2, w_1', w_1' and V_2 are all zero. At left the support ($x = 0$) u_1, u_2, w_1, w_2, w_1' and w_2' are continuous. Moreover, the deflection of the lower adherend is zero at the support, $w_2 = 0$. Also N_1, N_2, M_1, M_2 and V_1 are continuous at the support. In all this gives us 12 more conditions to fulfil at $x = 0$.

The free end ($x = -c$) is not subjected to any external loads. This means that the normal forces, N_1 and N_2, and the bending moments, M_1 and M_2, are all zero. However, in the present formulation, the shear stress in the interlayer is directly connected to the shear deformation of the interlayer, Eq. (13a), which may not be zero at a free end. Hence, the formulation does not allow for a zero interlayer shear stress at a free boundary. Due to equilibrium it also becomes impossible to guarantee vanishing of the shear forces, V_1 and V_2, since these are required to compensate for the non-zero shear stress at the free end of the interlayer, see Fig. 4b. There is no unambiguous way to split the spurious shear forces in the two adherends. Here, the shear forces are split in proportion to the bending stiffnesses of the adherends, i.e. $V_1(-c)/(E_1 h_1^3) = V_2(-c)/(E_2 h_2^3)$. In order to fulfil the condition of zero external vertical load at the free end, the total shear force, $\overline{V} = V_1 + V_2 + bt\tau$, is set to zero. With these six conditions at the left free end ($x = -c$), 12 conditions at the left support ($x = 0$) and six conditions at the loading point ($x = L/2$), a system of 24 equations is formed.

The fact that the model can only achieve approximate boundary condition at a free end might introduce spurious stresses. However, these are likely to be present only in the vicinity of the free end. The focus of the present paper is to obtain global measures, such as the load point compliance, which will not be affected by the end-effects to any measurable extent.

3.3.3. Solution and extraction of compliance and stresses

For the case of no overhang, the 12 integration constants may be used to form a 12×12 system of equations. If an overhang is present the 24 integration constants are determined from a 24×24 system of equations formed from the boundary conditions described previously. Some of the coefficients of the systems of equations contain quite a number of terms. Here, the MATLAB® symbolic tool box is used to form the coefficients symbolically. The system of equations is solved numerically using a MATLAB® built-in matrix inversion tool. Once the integration constants have been determined, the deformation of the interlayer is given by Eq. (17) or (22), depending on whether the configuration is balanced or unbalanced. The stresses in the interlayer are subsequently determined from Eqs. (4), (5) and (13), and the displacements of the adherends from Eqs. (25) and (26). Here, the compliance of the three-point flexure specimen, $C = w_1(L/2)/P$, is of special interest. The stress resultants, $N_{1,2}$, $M_{1,2}$ and $V_{1,2}$, are found from Eqs. (6), (7) and (28).

3.4. Stresses in the adherends

The axial normal stress in each adherend is given by Navier's formula

$$\sigma_i(x, z_i) = \frac{N_i(x)}{b h_i} + 12\frac{M_i(x)}{b h_i^3} z_i, \quad i = 1,2 \tag{29}$$

where z_1 and z_2 are coordinates in the vertical direction measuring the distance from the middle plane of each adherend, see Fig. 6. The shear stress in each adherend is determined from longitudinal equilibrium of 'cut-out' sections of the adherends, see Fig. 6

$$\tau_1(x,z_1) = -\int_{-h_1/2}^{z_1} \frac{\partial\sigma_1}{\partial x}(x,\tilde{z}_1)\mathrm{d}\tilde{z}_1, \quad \tau_2 = \int_{z_2}^{h_2/2} \frac{\partial\sigma_2}{\partial x}(x,\tilde{z}_2)\mathrm{d}\tilde{z}_2 \tag{30a,b}$$

Determination of the shear stress, τ_i, thus requires the derivative of σ_i, obtained by inserting the equilibrium Eqs. (1) and (3) into a differentiated Navier's formula (29). Integration according to Eq. (30) yields

$$\tau_i(x,\bar{z}_i) = \frac{1}{4}\left(3\bar{z}_i^2 \pm 2\bar{z}_i - 1\right)\tau(x) + \left(1-\bar{z}_i^2\right)\frac{3}{2}\frac{V_i(x)}{bh_i}, \quad i = 1,2 \tag{31}$$

where the positive/negative signs apply for the upper/lower adherend (i = 1, 2). Normalized coordinates, $\bar{z}_i = 2z_i/h_i$, have been introduced, i.e. $\bar{z}_i = \mp 1$ at the free outer surfaces, $\bar{z}_i = 0$ at the adherend centroid and $\bar{z}_i \pm 1$ at the interlayer/adherend interface, respectively. According to Eq. (31), the shear stress distribution in an adherend consists of one part proportional to the shear stress in the interlayer and another part proportional to the shear force in the adherend. It is seen that both parts satisfy the traction-free outer surfaces of the adherends, i.e. $\tau_i(x, \mp 1) = 0$. At the interlayer/adherend interface, the shear stress equals the shear stress in the interlayer, i.e. $\tau_i(x, \pm 1) = \tau(x)$, as expected. The shear stress in the adherends due to the transverse shear force is parabolically distributed, i.e. precisely as in classical beam theory (Gere and Timoshenko, 1984). Also the shear stress in the adherends due to the interlayer shear stress is parabolically distributed over the cross section. As expected, this part of the shear stress distribution has a zero resultant.

The transverse normal stress, σ_{zi} is determined from vertical equilibrium of the 'cut-out' pieces of the adherends, Fig. 6

$$\sigma_{z1}(x,z) = -\int_{-h_1/2}^{z_1} \frac{\partial\tau_1}{\partial x}(x,\tilde{z})\mathrm{d}\tilde{z}, \quad \sigma_{z2} = \int_{z_2}^{h_2/2} \frac{\partial\tau_2}{\partial x}(x,\tilde{z})\mathrm{d}\tilde{z} \tag{32a,b}$$

The derivative of the adherend shear stress, τ_i', is obtained by inserting Eqs. (2), (4) and (5) into a differentiated Eq. (31). Integration according to Eq. (32) yields

$$\sigma_{zi}(x,\bar{z}_i) = \frac{\sigma_s}{4}\left[\mp\bar{z}_i^3 \pm 3\bar{z}_i + 2\right] + \frac{\sigma_a h_i}{4t}\left[-\left(1+\frac{t}{h_i}\right)\bar{z}_i^3 \mp \bar{z}_i^2 + \left(1+3\frac{t}{h_i}\right)\bar{z}_i \pm \left(1+2\frac{t}{h_i}\right)\right], \quad i = 1,2 \tag{33}$$

Hence, the transverse normal stress in an adherend consists of two parts; one proportional to the symmetric part of the normal stress on the interlayer, σ_s, and another one proportional to the antisymmetric part, σ_a, cf. Eq. (4).

4. Solution for an incompressible interlayer

For the case of an incompressible interlayer (ν = 1/2) the effective Young's modulus, $\bar{E}$, is infinitely large, cf. Eq. (13b). A different solution procedure than in the previous section must then be followed. The consequence of the incompressibility is that the thickness stretch of the interlayer, w, is zero along the entire beam. According to Eq. (8b) this means that the deflection of the two adherends are identical, i.e. $w_1(x) \equiv w_2(x)$. This is utilized in the following derivation, where entities of adherend #1 are eliminated in favour of entities of adherend #2. The following dimensionless quantities are introduced:

$$\Sigma = \frac{E_1}{E_2}, \quad \eta = \frac{h_1}{h_2}, \quad \zeta = \frac{t}{h_2}. \tag{34a,b,c}$$

Identical deflections implicate that also the curvatures of the two adherends are identical, i.e. $w_1'' \equiv w_2''$. It then follows from Eq. (7) that the bending moments are related through

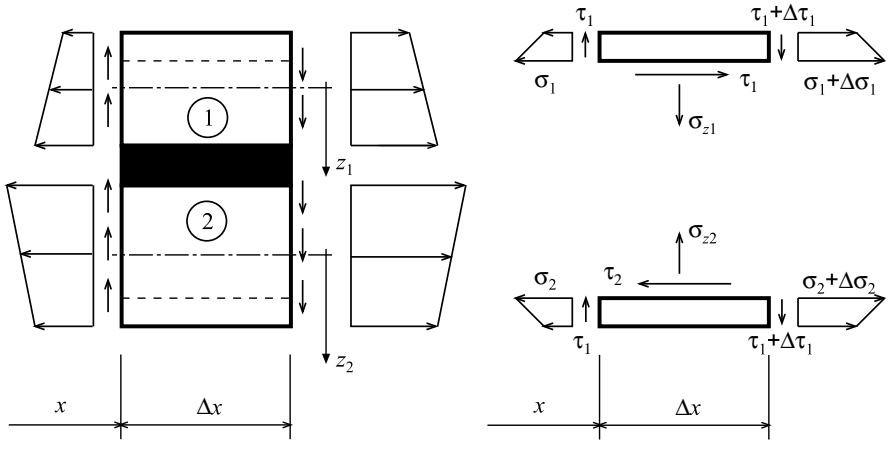

Fig. 6. Free body diagram for determination of stresses in adherends.

$$M_1(x) = \Sigma\eta^3 M_2(x) \tag{35}$$

Furthermore, longitudinal equilibrium requires that $N_1(x) \equiv -N_2(x)$. It then follows from Eq. (6):

$$u_1'(x) = -\Sigma^{-1}\eta^{-1}u_2'(x) \tag{36}$$

A relation between the shear forces and the bending moments is obtained from Eq. (3). By use of Eq. (35) it reads

$$V_1(x) = \eta V_2(x) + \eta(\Sigma\eta^2 - 1)M_2'(x) \tag{37}$$

Eqs. (35) and (37) show that for incompressible interlayers it is not possible to independently prescribe bending moments and shear forces on the two adherends.

All displacements and stress resultants of adherend #1 have now been eliminated. The derivation for symmetric beams presented by Alfredsson et al. (2008) is here generalized to the unsymmetric case. Hence, the deflection, w_2, and the longitudinal displacement, u_2, are eliminated to form an equation in the shear deformation of the interlayer. This leads to a second order differential equation (see Appendix C)

$$v''(x) - \kappa^2 v(x) = -\kappa^2 \bar{\tau} t/G \tag{38}$$

where

$$\bar{\tau} = \frac{6\overline{V}}{bh_2}\frac{1+\eta+2\zeta}{(\Sigma\eta^3+1)(1+\Sigma^{-1}\eta^{-1})+3(1+\eta+2\zeta)^2} \tag{39}$$

is the constant shear stress in the interlayer obtained by ordinary beam theory (Gere and Timoshenko, 1984), and

$$\kappa = \sqrt{\frac{(\Sigma\eta^3+1)(1+\Sigma^{-1}\eta^{-1})+3(1+\eta+2\zeta)^2}{\Sigma\eta^3+1}\frac{G}{E_2h_2t}} \tag{40}$$

A beam with symmetric overhang, i.e. $c > 0$ in Fig. 1, is considered. Due to symmetry, only the left part, $-c \leqslant x \leqslant L/2$, is studied. The general solution to Eq. (38) is

$$v(x) = \begin{cases} (H_1 e^{\kappa x} + H_2 e^{-\kappa x})\frac{\bar{\tau}}{k} & \text{for} \quad -c \leqslant x \leqslant 0 \\ (H_3 e^{\kappa x} + H_4 e^{-\kappa x} + 1)\frac{\bar{\tau}}{k} & \text{for} \quad 0 \leqslant x \leqslant L/2 \end{cases} \tag{41}$$

where $\bar{\tau}$ is given by Eq. (39) with $\overline{V} = P/2$. The absence of a constant term for the overhang portion in Eq. (41) reflects the fact that the total shear force, $\overline{V}$, is zero in the overhang part of the beam. The constants H_i ($i = 1, 2, 3$ and 4) are determined by conditions on v or v'. With prescribed end forces and moments, the following relation, obtained from Eqs. (6), (7), (8) and (11), can be used to form boundary conditions on v'

$$v'(x) = \frac{N_2(x)}{E_2bh_2} - \frac{N_1(x)}{E_1bh_1} - \frac{6(1+\zeta/\eta)M_1(x)}{E_1bh_1^2} - \frac{6(1+\zeta)M_2(x)}{E_2bh_2^2} \tag{42}$$

From this equation it also follows that not only v but also v' are continuous when no concentrated longitudinal forces or moments are applied to the adherends.

According to Eq. (42), the boundary conditions at the free left end is $v'(-c) = 0$. At midspan the shear deformation vanishes, i.e. $v(L/2) = 0$. Moreover, both v and v' must be continuous at the support, $x = 0$. With these four conditions, the integration constants become

$$H_1 = \frac{1}{2}\frac{e^{\kappa L/2} + e^{\kappa L/2} - 2}{e^{\kappa L/2} + e^{-\kappa(4c+L)/2}} \tag{43a}$$

$$H_2 = H_1 e^{-2\kappa c} = \frac{1}{2}\frac{e^{\kappa(L-4c)/2} + e^{-\kappa(4c+L)/2} - 2e^{-2\kappa c}}{e^{\kappa L/2} + e^{-\kappa(2c+L/2)}} \tag{43b}$$

$$H_3 = H_1 - \frac{1}{2} = \frac{1}{2}\frac{e^{-\kappa L/2} - e^{-\kappa(4c+L)/2} - 2}{e^{\kappa L/2} + e^{-\kappa(4c+L)/2}} \tag{43c}$$

$$H_4 = H_2 - \frac{1}{2} = \frac{1}{2}\frac{e^{\kappa(L-4c)/2} - e^{\kappa L/2} - 2e^{-\kappa c}}{e^{\kappa L/2} + e^{-\kappa(4c+L)/2}} \tag{43d}$$

The longitudinal force, N_2, is obtained by integration of Eq. (1b)

$$N_2(x) = b\int_{-c}^{x} \tau[v(\tilde{x})]\mathrm{d}\tilde{x} \tag{44}$$

The bending moment in the adherends is determined from equilibrium and Eq. (35)

$$(\Sigma\eta^3+1)M_2(x) = \begin{cases} -\frac{1}{2}(h_1+h_2+2t)N_2(x) & \text{for} \quad -c \leqslant x \leqslant 0 \\ \frac{1}{2}Px - \frac{1}{2}(h_1+h_2+2t)N_2(x) & \text{for} \quad 0 \leqslant x \leqslant L/2 \end{cases} \tag{45}$$

With the bending moment determined, the deflection, $w_2(x)$, is determined by integration of Eq. (7b). With the boundary conditions, $w_2(0) = 0$ and $w'_2(L/2) = 0$, the compliance, $C_{oh} = w_2(L/2)/P$, takes the form

$$\frac{C_{oh}}{C_{bt}} = 1 + \frac{(1+\eta+2\zeta)^2}{(\Sigma\eta^3+1)(1+\Sigma^{-1}\eta^{-1})}\frac{36}{\kappa^3 L^3}\left[H_3\{e^{\kappa L/2}(2-\kappa L)-2\} + H_4\{2-e^{-\kappa L/2}(2+\kappa L)\}\right] \tag{46}$$

where C_{bt} is the compliance of a three-layer beam according to ordinary beam theory

$$C_{bt} = \frac{L^3}{4E_2 b h_2^3}\frac{1+\Sigma^{-1}\eta^{-1}}{3(1+\eta+2\zeta)^2+(\Sigma\eta^3+1)(1+\Sigma^{-1}\eta^{-1})} \tag{47}$$

Eq. (46) is a generalization of the compliance derived for symmetric beams in Alfredsson et al. (2008). The compliance, C_{oh}, is a complex function of the geometry and material properties of the adherends and interlayer. In order to gain further insight, beams without and with overhang are discussed separately below.

4.1. Beams without overhang

For beams without overhang ($c = 0$), Eq. (46) yields

$$\frac{C}{C_{bt}} = 1 + \frac{36(1+\eta+2\zeta)^2}{(\Sigma\eta^3+1)(1+\Sigma^{-1}\eta^{-1})}\left[\frac{1}{\kappa^2 L^2} - \frac{2}{\kappa^3 L^3}\tanh\left(\frac{\kappa L}{2}\right)\right] \tag{48}$$

There are two effects of the interlayer thickness on the compliance: (i) With increasing interlayer thickness the beam thickness increases, which tends to reduce the global compliance. This is termed 'the thickness effect'. If only the thickness effect is accounted for, the compliance equals C_{bt}, Eq. (47), i.e. the compliance predicted by ordinary beam theory; (ii) With increasing interlayer thickness the shear flexibility of the interlayer increases, which will increase the global compliance. This is called 'the flexibility effect' in Alfredsson et al. (2008). The flexibility effect is isolated by assuming that the interlayer thickness is small compared to the thickness of the adherends, i.e. $\zeta \ll 1$, Eq. (34c). For this case the global compliance, C, becomes

$$\frac{C}{C_0} = 1 + f(\beta)F(\Sigma,\eta) \tag{49}$$

where C_0 is the compliance when the two adherends are rigidly connected with a layer of zero thickness

$$C_0 = C_{bt}(\zeta = 0) = \frac{L^3}{4E_2 b h_2^3}\frac{1+\Sigma^{-1}\eta^{-1}}{3(1+\eta)^2+(\Sigma\eta^3+1)(1+\Sigma^{-1}\eta^{-1})} \tag{50}$$

The function $f(\beta)$ quantifies the decoupling of the adherends that occurs by shear deformation of the interlayer

$$f(\beta) = \frac{3}{2}\beta\left[1 - \sqrt{\frac{\beta}{2}}\tanh\left(\sqrt{\frac{2}{\beta}}\right)\right] \tag{51}$$

where β is a de-coupling parameter

$$\beta = \frac{8(\Sigma\eta^3+1)}{3(1+\eta)^2+(\Sigma\eta^3+1)(1+\Sigma^{-1}\eta^{-1})}\frac{E_2}{G}\left(\frac{h_2}{L}\right)^2\zeta \tag{52}$$

The factor F in Eq. (49) is defined in terms of the adherend parameters Σ and η as

$$F(\Sigma,\eta) = \frac{3(1+\eta)^2}{(\Sigma\eta^3+1)(1+\Sigma^{-1}\eta^{-1})} \tag{53}$$

This factor describes the relative increase of the compliance from a fully coupled to a fully decoupled state (G varies from ∞ to 0). Fig. 7 displays the variation of F with the material and geometry factors, $\bar{\Sigma}$ and $\bar{\eta}$, defined by

$$\bar{\Sigma} = \frac{E_1}{E_1+E_2}, \quad \bar{\eta} = \frac{h_1}{h_1+h_2} \tag{54a,b}$$

Fig. 7 shows that the maximum of F ($F_{max} = 3$) is attained for balanced configurations, i.e. $\Sigma\eta^2 = 1$. The curves are symmetric with respect to $\bar{\Sigma} = 1/2$ and $\bar{\eta} = 1/2$, which shows that the compliance remains the same if the adherends #1 and #2 are switched.

Fig. 8 shows the decoupling function, f, plotted versus the decoupling factor, β (Eqs. (51) and (52)). β is varied by (for example) varying the layer shear modulus, G. When $G \approx 0$, $\beta \to \infty$, and the two adherends become effectively disconnected; $C \to (1+F)C_0 \equiv C_{slide}$, where C_{slide} is the compliance for two beams stacked frictionless on top of each other. For a layer that is rigid in shear, $G \to \infty$, $f(\beta)$ approaches zero, and the two adherends become fully coupled ($C = C_0$).

To relate the "fully coupled" and "fully decoupled" asymptotic states in terms of values of the parameter β (Fig. 8), we require 99 and 1% increases, respectively, of the maximum possible increase of the compliance (Eq. (49)). These extremes

correspond, respectively, to $f = 0.99$ and 0.01 in Eq. (51), and β values of 79 (fully decoupled) and 0.0071 (fully coupled), respectively.

4.2. Beams with overhang

As shown in the previous publication (Alfredsson et al., 2008), the presence of an overhang ($c > 0$) will restrict sliding deformations of the adherends, and reduce the global compliance, i.e. $C_{oh} < C$. However, the global compliance cannot be reduced indefinitely. For large values of the overhang the global compliance, C_{oh} in Eq. (46), approaches an asymptotic value

$$\frac{C_\infty}{C_{bt}} = 1 + \frac{(1+\eta+2\zeta)^2}{(\Sigma\eta^3+1)(1+\Sigma^{-1}\eta^{-1})}\frac{36}{\kappa^3 L^3}[\kappa L - 3 - e^{\kappa L} + 4e^{-\kappa L/2}] \tag{55}$$

For $\kappa c > 3$ the limit value of the compliance, C_∞, is a very good approximation to C_{oh}, regardless of the span length. From Eqs. (40) and (55) it follows that the limit value of the overhang is obtained at an overhang length of

$$c_\infty = 3\sqrt{\frac{E_2 h_2 t}{G}\frac{\Sigma\eta^3+1}{3(1+\eta+2\zeta)^2+(\Sigma\eta^3+1)\left(1+\Sigma^{-1}\eta^{-1}\right)}} \tag{56}$$

Hence, for any overhang length greater than c_∞, the compliance will be very close to the limit value of the compliance, C_∞.

5. Applied results

In order to study the influence of material unsymmetry on the compliance of the asymmetric beams, parametric analysis is conducted. A specific beam is considered as a baseline. The top adherend is given the effective properties of a stiff surface

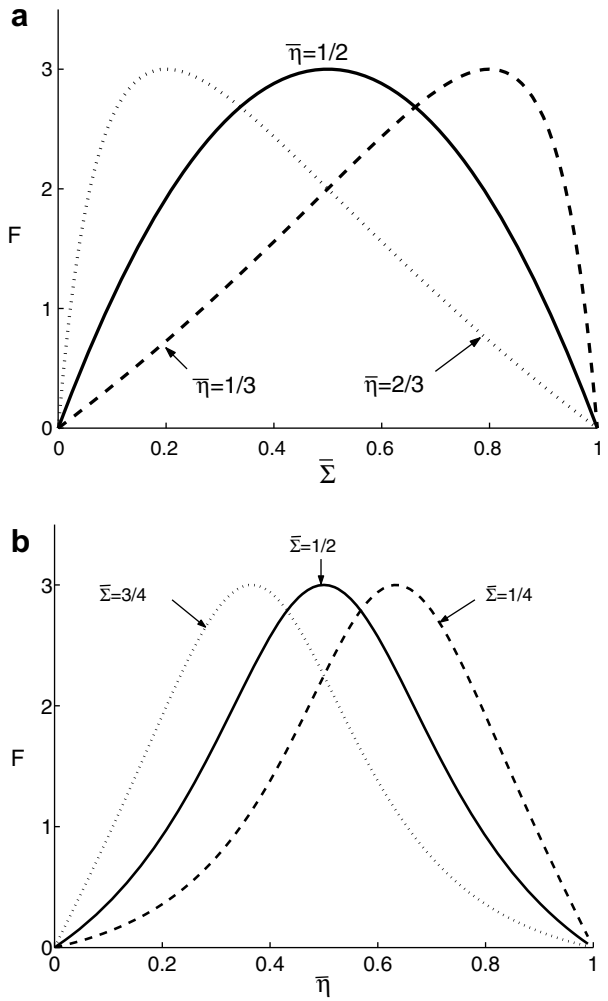

Fig. 7. Variation of function F: (a) with $\bar{\Sigma}$ for different values of $\bar{\eta}$, and (b) with $\bar{\eta}$ for different values of $\bar{\Sigma}$.

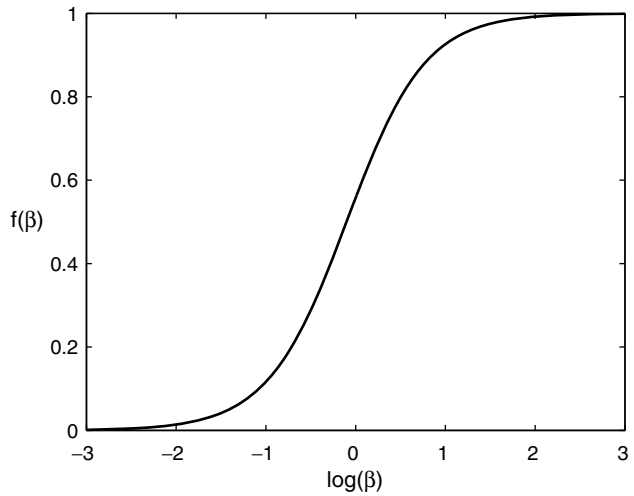

Fig. 8. Variation of function f with de-coupling parameter, β.

layer representative for steel ($E_1 = 200$ GPa, $\nu = 0.3$, $h_1 = 15$ mm). The lower adherend is of equal thickness as the upper adherend but much less stiff, representative for a glass fiber composite loaded in the fiber direction ($E_2 = 20$ GPa, $\nu = 0.1$, $h_2 = 15$ mm). The adherends are joined by a rubber interlayer ($G = 3$ MPa, $\nu = 0.49$) and the layer thickness is varied. Three span lengths are studied; $L = 0.2$, 0.5 and 1 m, while the overhang is kept constant ($c = 50$ mm).

To achieve insight in the response of the beam configurations considered, the variation of the decoupling parameter β, cf. Eq. (52) is examined. Fig. 9 shows the variation of β with the interlayer thickness for span lengths, $L = 0.2$, 0.5 and 1 m. In the interval of the interlayer thickness studied, $0.1 \leqslant t \leqslant 10$ mm, full decoupling is expected only for the shortest span length, $L = 0.2$ m, at an interlayer thickness close to 10 mm. However, overall, all three configurations in Fig. 9, are far from fully coupled. β falls in the intervals {0.91–91}, {0.146–14.6} and {0.0365–3.65} for $L = 0.2$, 0.5 and 1 m, respectively. According to Eq. (51) and Fig. 8, these values of β correspond to the following values of the function f appearing in Eq. (49); {0.53–0.99}, {0.16–0.95} and {0.047–0.82}. For the present combination of adherends the factor F defined in Eq. (53) becomes, $F = 0.99$, which implies that the maximum possible increase of the compliance over a fully coupled beam is 99%. For the span lengths, $L = 0.2$, 0.5 and 1 m, Eq. (49) reveals that the compliance is expected to increase by a maximum of 98, 94 and 81% as compared to a fully coupled beam with zero interlayer thickness. These values are approximate and overestimate the compliance increase since they are based on a negligible interlayer thickness. For some of the geometries considered the interlayer thickness is comparable to the thickness of the adherends.

Results for the influence of the finite thickness of the layer on the compliance are shown in Fig. 10. The solid lines represent the results for incompressible interlayers ($\nu = 0.5$) and the dotted lines the results for a slightly compressible interlayer ($\nu = 0.49$). For short beams with thick interlayers, the compliance predicted assuming incompressibility falls below the one obtained assuming compressibility. The effect of the compression on the compliance is smaller for large span lengths.

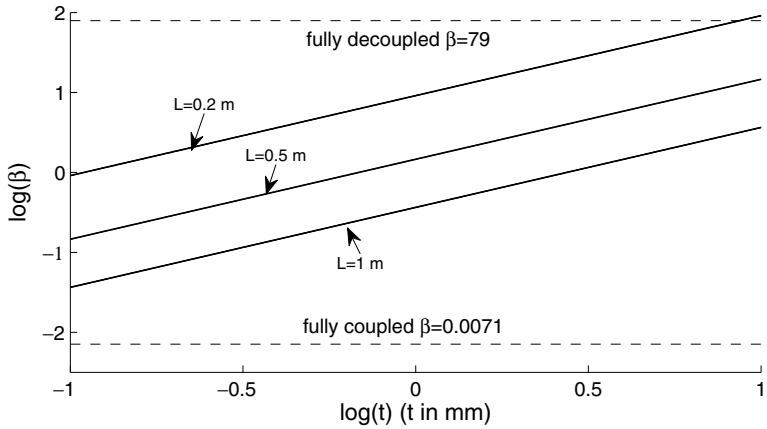

Fig. 9. Parametric study of steel/rubber/glass beam. Decoupling factor, β, is shown as a function of rubber layer thickness for different span lengths. Limits for full decoupling/coupling are indicated. Data: $E_1 = 200$ GPa, $E_2 = 20$ GPa, $h_1 = h_2 = 15$ mm, $c = 50$ mm, $G = 3$ MPa, $\nu = 0.49$.

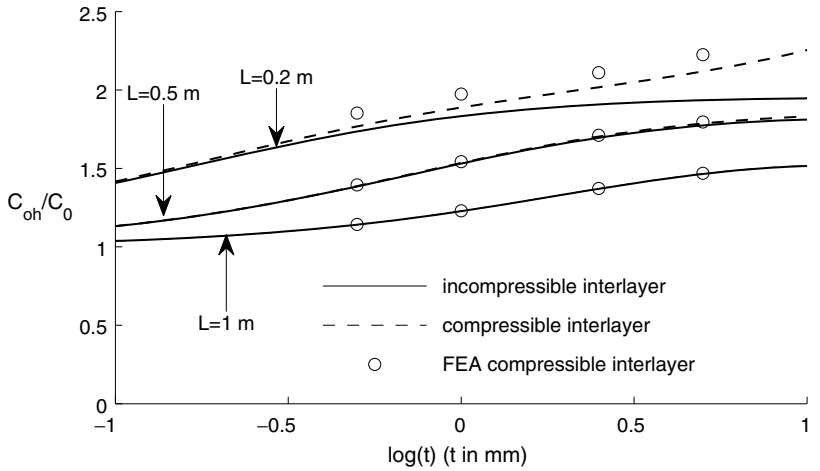

Fig. 10. Parametric study of steel/rubber/glass beam. Normalized compliance values are shown as a function of rubber layer thickness for different span lengths. Solid curves show values according to incompressible solution, dashed curves according to compressible solution and circles according to FE-simulations. Data: E_1 = 200 GPa, E_2 = 20 GPa, $h_1 = h_2$ = 15 mm, c = 50 mm, G = 3 MPa, ν = 0.49.

The results above are compared to those obtained from a finite element model with ν = 0.49 where the adherends as well as the interlayer are modeled with continuum elements. For details of the FE-model the reader is referred to (Alfredsson et al., 2008), where similar simulations are performed on symmetric beams. The results of the FE-model are indicated by the discrete points in Fig. 10. Since less constraints are introduced in the FE-model, it yields compliance values which slightly exceed those from the analytical beam theory models, but the difference is overall quite small. It is also seen that the increasing trend of the compliance for large values of the interlayer thickness is well captured.

6. Experiments

The validity of the analyses presented above was examined by testing unsymmetric beams with a flexible interlayer in three-point flexure. The beams consisted of dissimilar aluminum adherends connected by an adhesively bonded rubber layer. Table 1 details the thicknesses and widths of the adherends and the rubber layer. The tests were conducted on asymmetric beams at a constant span length, L = 20.3 cm, and at overhang lengths; c = 2.54, 5.08, 7.62, 10.2 and 12.7 cm. Such a set of beam configurations was achieved by testing the beams with the longest overhang first. After the test, the beam was removed from the fixture, and sections of 2.54 cm length were cut from each end. This procedure was repeated until the overhang length was 2.54 cm on each side. Details of specimen preparation, testing and data reduction for the beam compliance are presented in the earlier publication by Alfredsson et al. (2008). The publication also details measurement of the shear modulus (G) of the rubber layer; G = 3.11 MPa. Young's modulus ($E_{1,2}$) of the aluminum adherends was measured from a three-point flexure test on one of the adherends before assembly of the layered beam. This test provided $E_{1,2}$ = 70 GPa, in good agreement with handbook values.

Fig. 11 shows compliance of the beam vs. overhang length. The open circles represent experimental test data determined as described above and the continuous curve represents predictions from Eq. (46). It is verified that the presence of an overhang reduces the compliance, and the test data are in very good agreement with the beam model predictions.

7. Concluding remarks

Layer-wise analysis of the stresses and deflection of a three-layer beam configuration consisting of two dissimilar orthotropic adherends of different thicknesses that are joined together by a flexible interlayer has been presented. The adherends are assumed to deform according to beam theory and the interlayer may deform in the thickness direction and in shear. The

Table 1
Dimensions of aluminum adherends and rubber interlayers used in experimental test program

Beam #	h_1 (mm)	h_2 (mm)	b_1 (mm)	b_2 (mm)	t (mm)
1	6.53	6.22	51.0	50.7	0.76
2	6.53	12.6	51.0	51.0	0.76
3	6.53	12.6	51.9	51.9	3.0

model is similar to the model presented by Frostig et al. (1991), although the present solution reveals a more complex interaction between extensional and shear stresses in the flexible interlayer.

Both compressible and incompressible interlayers are considered in the formulation and analytical solutions are obtained for the case of three-point flexure loading. A closed-form solution is presented for the case of an incompressible interlayer and equations expressing conditions on mechanical coupling of the adherends by the interlayer are derived in dimensionless form. The analysis revealed that configurations where the moduli and thicknesses of the adherends (1 and 2) are matched

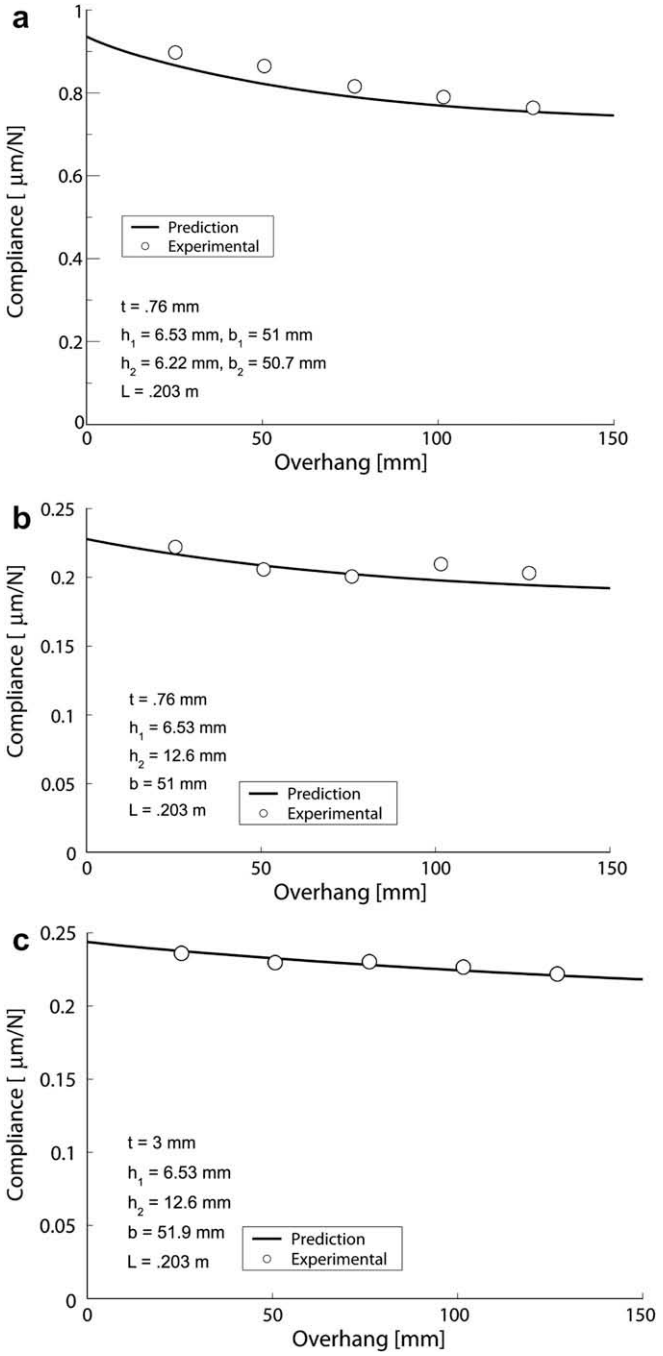

Fig. 11. Compliance as a function of overhang for unsymmetric beam configurations with a rubber layer. Data: $L = .203$ m. $E_1 = E_2 = 70$ GPa, $G = 3.3$ MPa, $\nu = 0.49$, (a) $t = .76$ mm, $h_1 = 6.53$ mm, $h_2 = 6.22$ mm, $b = 51.0$ mm, (b) $t = .76$ mm, $h_1 = 6.53$ mm, $h_2 = 12.6$ mm, $b = 51.0$ mm, (c) $t = 3$ mm, $h_1 = 6.53$ mm, $h_2 = 12.6$ mm, $b = 51.9$ mm.

according to $E_1h_1^2 = E_2h_2^2$ (balanced) have the largest potential for compliance increase by reduction of the interlayer shear modulus.

The analytical solutions agreed closely with finite element results. Experimental measurements of compliance of various unsymmetric beams consisting of aluminum adherends separated by a rubber interlayer were performed over a range of overhang lengths in order to validate the analysis. Excellent agreement between measured and predicted compliance values was observed.

Acknowledgements

The authors would like to acknowledge funding from the Army Research Laboratory (Co-operative agreement # DAAD19-01-2-0005) for the Materials Center of Excellence in Composites established at the University of Delaware Center for Composite Materials.

Appendix A. Elimination of displacements for a compressible interlayer

First the individual longitudinal beam displacements are eliminated by combining Eqs. (1) and (6)

$$u_1''(x) = -\frac{\tau(x)}{E_1h_1}, \quad u_2''(x) = \frac{\tau(x)}{E_2h_2}, \tag{A1a, b}$$

Subtraction of Eq. (A1a) from (A1b) and using Eq. (8a) gives

$$u''(x) = \left(\frac{1}{E_1h_1} + \frac{1}{E_2h_2}\right)\tau(x) \tag{A2}$$

The individual vertical beam displacements are eliminated by first combining Eqs. (2), (3) and (7)

$$w_1^{IV}(x) = \frac{6}{E_1h_1^2}\tau'(x) + \frac{12}{E_1h_1^3}\sigma_1(x) \tag{A3a}$$

$$w_2^{IV}(x) = \frac{6}{E_2h_2^2}\tau'(x) - \frac{12}{E_2h_2^3}\sigma_2(x) \tag{A3b}$$

Subtraction of Eq. (A3a) from Eq. (A3b) and using Eqs. (4), (5) and (8b) gives

$$w^{IV}(x) = 6\left(\frac{1+\frac{t}{h_2}}{E_2h_2^2} - \frac{1+\frac{t}{h_1}}{E_1h_1^2}\right)\tau'(x) - 12\left(\frac{1}{E_1h_1^3} + \frac{1}{E_2h_2^3}\right)\sigma_s(x) \tag{A4}$$

This is Eq. (12a) in the main text. Eq. (A3) yield

$$\frac{1}{2}(h_1+t)w_1^{IV}(x) = 3\frac{1+\frac{t}{h_1}}{E_1h_1}\tau'(x) + 6\frac{1+\frac{t}{h_1}}{E_1h_1^2}\sigma_1(x) \tag{A5}$$

$$\frac{1}{2}(h_2+t)w_2^{IV}(x) = 3\frac{1+\frac{t}{h_2}}{E_2h_2}\tau'(x) - 6\frac{1+\frac{t}{h_2}}{E_2h_2^2}\sigma_2(x) \tag{A6}$$

By use of Eq. (A2) we may write

$$3\left(\frac{1}{E_1h_1} + \frac{1}{E_2h_2}\right)\tau'(x) = 4\left(\frac{1}{E_1h_1} + \frac{1}{E_2h_2}\right)\tau'(x) - u'''(x) \tag{A7}$$

From Eqs. (11), (A5), (A6) and (A7) it follows that:

$$v'''(x) = 4\left(\frac{1+\frac{3}{2}\frac{t}{h_1}+\frac{3}{4}\left(\frac{t}{h_1}\right)^2}{E_1h_1} + \frac{1+\frac{3}{2}\frac{t}{h_2}+\frac{3}{4}\left(\frac{t}{h_2}\right)^2}{E_2h_2}\right)\tau'(x) + 6\left(\frac{1}{E_1h_1^2} - \frac{1}{E_2h_2^2}\right)\sigma_s(x) \tag{A8}$$

which is Eq. (12b) in the main text.

Appendix B. Displacements of the adherends for a compressible interlayer

General expressions for the deflections of the adherends can be derived from Eq. (A3) with (13) and (15a,b),

$$w_1^{IV}(x) = A_1v'(x) + B_1w(x), \quad w_2^{IV}(x) = A_2v'(x) - B_2w(x) \tag{B1a, b}$$

Here, Eq. (14) can be used to obtain alternative expressions for $v'(x)$ and $w(x)$

$$v' = \frac{Bv''' - Dw^{IV}}{BC - AD} = \frac{B^2 v^V - BDw^{VI} - D(BC - AD)w^{IV}}{(BC - AD)^2} \tag{B2a}$$

$$w = \frac{Av''' - Cw^{IV}}{BC - AD} = \frac{ABv^V - ADw^{VI} - C(BC - AD)w^{IV}}{(BC - AD)^2} \tag{B2b}$$

Next, these expressions are inserted into Eqs. (B1), and integrated four times. The result is

$$w_1(x) = A_1 \frac{B^2 v' - BDw'' - D(BC - AD)w}{(BC - AD)^2} + B_1 \frac{ABv' - ADw'' - C(BC - AD)w}{(BC - AD)^2} + I_0 \frac{x^3}{L^3} + I_1 \frac{x^2}{L^2} + I_2 \frac{x}{L} + I_3 \tag{B3a}$$

$$w_2(x) = A_2 \frac{B^2 v' - BDw'' - D(BC - AD)w}{(BC - AD)^2} - B_2 \frac{ABv' - ADw'' - C(BC - AD)w}{(BC - AD)^2} + \bar{I}_0 \frac{x^3}{L^3} + \bar{I}_1 \frac{x^2}{L^2} + \bar{I}_2 \frac{x}{L} + \bar{I}_3 \tag{B3b}$$

where eight new integration constants appear. Now, the difference of these two expressions is formed. By use of Eq. (15a,b) it follows:

$$w_2(x) - w_1(x) = w(x) + (\bar{I}_0 - I_0)\frac{x^3}{L^3} + (\bar{I}_1 - I_1)\frac{x^2}{L^2} + (\bar{I}_2 - I_2)\frac{x}{L} + (\bar{I}_3 - I_3) \tag{B4}$$

According to the definition of the deformation of the interlayer, $w(x)$, Eq. (8b), we must have

$$(\bar{I}_0 - I_0)\frac{x^3}{L^3} + (\bar{I}_1 - I_1)\frac{x^2}{L^2} + (\bar{I}_2 - I_2)\frac{x}{L} + (\bar{I}_3 - I_3) = 0 \tag{B5}$$

and thus

$$\bar{I}_0 = I_0, \quad \bar{I}_1 = I_1, \quad \bar{I}_2 = I_2, \quad \bar{I}_3 = I_3 \tag{B6a-d}$$

General solutions of the axial displacements in the adherends will be derived. From Eq. (A1) with (13) and (15c)

$$u_1''(x) = -\frac{1}{4}\bar{C}_1 v(x), \quad u_2''(x) = +\frac{1}{4}\bar{C}_2 v(x) \tag{B7a, b}$$

Eq. (B2a) is integrated and combined with Eqs. (22) to obtain an expression for the shear deformation $v(x)$

$$v = \frac{Bv'' - Dw'''}{BC - AD} + K_7 \tag{B8}$$

Next, this expressions is inserted into Eq. (B7) and integrated twice

$$u_1(x) = -\frac{1}{4}\bar{C}_1 \left[\frac{Bv - Dw'}{BC - AD} + \frac{1}{2}K_7 x^2\right] + \bar{I}_4 \frac{x}{L} + I_5 \tag{B9a}$$

$$u_2(x) = +\frac{1}{4}\bar{C}_2 \left[\frac{Bv - Dw'}{BC - AD} + \frac{1}{2}K_7 x^2\right] + \bar{I}_4 \frac{x}{L} + \bar{I}_5 \tag{B9b}$$

The integration constants, $I_{4,5}$ and $\bar{I}_{4,5}$ are not independent. Their interrelation can be revealed by consideration of the shear deformation $v(x)$. Substitution of Eqs. (B3) and (B9) into Eqs. (8a) and (11) yields

$$v(x) = \frac{Bv'' - Dw'''}{BC - AD} + \left[\frac{1}{8}\bar{C}L^2 K_7 + \frac{3}{2}\frac{h_1 + h_2 + 2t}{L} I_0\right]\frac{x^2}{L^2} + \left[\bar{I}_4 - I_4 + \frac{h_1 + h_2 + 2t}{L} I_1\right]\frac{x}{L} + \left[\bar{I}_5 - I_5 + \frac{1}{2}\frac{h_1 + h_2 + 2t}{L} I_2 + \frac{1}{4}\frac{B\bar{C}}{BC - AD} K_7\right] \tag{B10}$$

According to Eqs. (B8) and (B10), we must have

$$\left[\frac{1}{8}\bar{C}L^2 K_7 + \frac{3}{2}\frac{h_1 + h_2 + 2t}{L} I_0\right]\frac{x^2}{L^2} + \left[\bar{I}_4 - I_4 + \frac{h_1 + h_2 + 2t}{L} I_1\right]\frac{x}{L} + \left[\bar{I}_5 - I_5 + \frac{1}{2}\frac{h_1 + h_2 + 2t}{L} I_2 + \frac{1}{2}\frac{B\bar{C}}{BC - AD} K_7\right] = K_7 \tag{B11}$$

Thus, the integration constants are interrelated through

$$I_0 = -\frac{1}{12}\frac{\overline{C}L^3}{h_1+h_2+2t}K_7, \quad \bar{I}_4 = I_4 - \frac{h_1+h_2+2t}{L}I_1 \tag{B12a, b}$$

$$\bar{I}_5 = I_5 - \frac{1}{2}\frac{h_1+h_2+2t}{L}I_2 + \left[1 - \frac{1}{4}\frac{B\overline{C}}{BC-AD}\right]K_7 \tag{B12c}$$

Insertion of Eqs. (B6) and (B12) into Eqs. (B3) and (B9) gives Eqs. (25) and (26) in the main text.

Appendix C. Elimination of displacements for incompressible interlayers

The relations in Eqs. (35)–(38) can now be used to obtain a solution for the case of an incompressible interlayer. Eqs. (2) and (4) describing vertical equilibrium of the adherends and the interlayer can be combined using Eqs. (4a) and (5). The result is

$$V_1'(x) + V_2'(x) + bt\tau'(x) = 0 \tag{C1}$$

Integration yields

$$V_1(x) + V_2(x) + bt\tau(x) = \overline{V}(x) \tag{C2}$$

where $\overline{V}$ is the total shear force transmitted by the cross section. This equation can also be obtained from vertical equilibrium, Fig. 4b. For the present three-point flexure case the total shear force is piecewise constant, i.e. $\overline{V}(x) = \pm P/2$, where the plus/minus-sign refer to the left/right part of the system.

Combination of Eqs. (37) and (C2) with use of Eqs. (1b), (6b) and (7b) yields

$$(\Sigma\eta^3+1)w_2'''(x) - \frac{6}{h_2^3}(1+\eta+2\zeta)u_2'' = -\frac{12\overline{V}}{E_2 b h_2^3} \tag{C3}$$

Use of Eqs. (11) and (36) transforms Eq. (C3) into a relation between the second derivatives of u_2 and v

$$\left[(\Sigma\eta^3+1)\left(1+\Sigma^{-1}\eta^{-1}\right) + 3(1+\eta+2\zeta)^2\right]u_2''(x) = (\Sigma\eta^3+1)v''(x) + \frac{6\overline{V}}{E_2 b h_2^3}(1+\eta+2\zeta) \tag{C4}$$

With the second derivative of u_2 from Eq. (C4) in the equation obtained by combining Eqs. (1b) and (6b), the following equation relating shear deformation and shear stress is found

$$(\Sigma\eta^3+1)E_2 h_2 v''(x) = \left[(\Sigma\eta^3+1)\left(1+\Sigma^{-1}\eta^{-1}\right) + 3(1+\eta+2\zeta)^2\right][\tau(x) - \overline{\tau}] \tag{C5}$$

where

$$\overline{\tau} = \frac{6\overline{V}}{bh_2}\frac{1+\eta+2\zeta}{(\Sigma\eta^3+1)\left(1+\Sigma^{-1}\eta^{-1}\right) + 3(1+\eta+2\zeta)^2} \tag{C6}$$

The equation is in agreement with the constant shear stress in the interlayer predicted by ordinary beam theory (Gere and Timoshenko, 1984).

Introduction of the constitutive relation, Eq. (13a), into (C5) yields the following differential equation

$$v''(x) - \kappa^2 v(x) = -\kappa^2\overline{\tau}t/G \tag{C7}$$

with

$$\kappa = \sqrt{\frac{(\Sigma\eta^3+1)\left(1+\Sigma^{-1}\eta^{-1}\right) + 3(1+\eta+2\zeta)^2}{\Sigma\eta^3+1}\frac{G}{E_2 h_2 t}} \tag{C8}$$

Eqs. (C6), (C7) and (C8) are identical to Eqs. (39), (38) and (40) in the main text.

References

Alfredsson, K.S., Bogetti, T.A., Carlsson, L.A., Gillespie, J.W., Yiournas, A., 2008. Flexure of beams with an interlayer – symmetric beams with orthotropic adherends. J. Mech. Mater. Struct. 3 (1), 45–62.

Alfredsson, K.S., Högberg, J.L., 2008. A closed-form solution to statically indeterminate adhesive joint problems – exemplified on ELS-specimens. Int. J. Adhes. Adhes. 28, 350–361.

Bigwood, D.A., Crocombe, A.D., 1989. Elastic analysis and engineering design formulae for bonded joints. Int. J. Adhes. Adhes. 9, 229–242.

Cornell, R.W., 1953. Determination of stresses in cemented lap joints. J. Appl. Mech. 20 (3), 355–364.

Davila, C.G., Chen, T.-K., 2000. Advanced modeling strategies for the analysis of tile-reinforced composite armor. Appl. Compos. Mater. 7, 51–68.

Frostig, Y., Baruch, M., Vilnay, O., Sheinman, I., 1991. Bending of nonsymmetric sandwich beams with transversely flexible core. J. Eng. Mech. 117 (9), 1931–1952.

Frostig, Y., Baruch, M., Vilnay, O., Sheinman, I., 1992. High-order theory for sandwich-beam behavior with transversely flexible core. J. Eng. Mech. 118 (5), 1026–1043.
Frostig, Y., 2003. Classical and high-order computational models in the analysis of modern sandwich panels. Comp. Part B 34, 83–100.
Gere, J.M., Timoshenko, S.P., 1984. Mechanics of Materials. Brookes/Cole Engineering Division, Monterey.
Goland, M., Reissner, E., 1944. The stresses in cemented joints. J. Appl. Mech. 66, A17–A27.
Hart-Smith, L.J., 1973. Adhesive-bonded single-lap joints. NASA Report, CR-112236.
Hohe, J., Librescu, L., Oh, S.Y., 2006. Dynamic buckling of flat and curved sandwich panels with transversely compressible core. Compos. Struct. 74, 10–24.
Klarbring, A., 1991. Derivation of a model of adhesively bonded joints by the asymptotic expansion method. Int. J. Eng. Sci. 29, 493–512.
Kristensen, R.F., Nielsen, K.L., Mikkelsen, L.P., 2008. Numerical studies of shear damped composite beam using a constrained damping layer. Compos. Struct. 83 (3), 304–311.
Mahdi, S., Gillespie Jr., J.W., 2004. Finite element analysis of tile-reinforced composite structural armor subjected to bending loads. Comp. Part B 35, 57–71.
Nayak, A.K., Shenoi, R.A., Moi, S.S.J., 2004. Transient response of composite sandwich plates. Comp. Struct. 64, 249–267.
Råde, L., Westergren, B., 1990. Beta – Handbook of Methematics. Studentlitteratur, Lund.
Reddy, J.N., 1984. A simple higher-order theory for laminated composite plates. J. Appl. Mech. 51, 745–752.
Timoshenko, S.P., Woinowsky-Krieger, S., 1959. Theory of Plates and Shells. McGraw-Hill, New York.
Whitney, J.M., 1987. Structural Analysis of Laminated Anisotropic Plates. Technomic, Lancaster.